Brief Communication: Monitoring impending slope failure with very high-resolution space borne Synthetic Aperture Radars

Andrea Manconi[1,2], Yves Bühler[1,2], Andreas Stoffel[1,2], Johan Gaume[1,2,3], Qiaoping Zhang[4], Valentyn Tolpekin[4]

[1] WSL Institute for Snow and Avalanche Research SLF, Flüelastrasse 11, CH-7260 Davos Dorf, Switzerland
[2] Climate Change, Extremes and Natural Hazards in Alpine Regions Research Centre CERC
[3] Institute for Geotechnical Engineering, ETH Zürich, Switzerland
[4] ICEYE Oy, Maarintie 6, 02150 Espoo, Finland

Correspondence to: Andrea Manconi (andrea.manconi@slf.ch)

Abstract. We demonstrate how high spatial and temporal resolution spaceborne synthetic aperture radar (SAR) imagery can improve slope deformation monitoring. We process ICEYE data over the Brienz/Brinzauls slope instability in the Swiss Alps, where a catastrophic failure occurred on June 15th, 2023. Image correlation applied to retrieve surface velocities shows results comparable to in-situ measurements. Pre- and post-failure acquisitions used to map areas invaded by debris and to compute volumetric changes associated are in good agreement with photogrammetric data. This study sets the baseline for new-generation satellite SAR data aimed at providing timely information in landslide early warning scenarios.

1 Introduction

The availability of spaceborne Synthetic Aperture Radar (SAR) sensors has considerably increased in recent years due to launch of numerous missions, a trend expected to continue. This scenario offers new options for the systematic use of SAR datasets in numerous applications related to natural hazards. For what concerns slope stability analyses, thanks to the ESA Copernicus Sentinel-1 mission, the applications have progressively migrated from classic surveys, in the form of local and/or regional scale processing efforts for inventorying purpose and/or for back analyses of case studies, to systematic/operational monitoring solutions (Bianchini et al., 2021). Several limitations remain, however, especially when the surface displacements sharply accelerate and the probability of slope failure increases (Manconi, 2021). New generation SAR missions promise to be a game changer due to the massive technological improvement introduced, reducing the cost of production and the size of satellites and sensors, thus allowing for the space missions providing a more frequent revisit (Sigmundsson et al., 2024).

In this work, we show the results of a pilot study performed during the crisis associated with the acceleration of the Brienz/Brinzauls slope instability (hereinafter referred to as Brienz), located in the Swiss alps, culminating in a failure on June 15, 2023, which accumulated ~1.2 Mm^3 of debris material very close to the village. There, surface velocities increased consistently since 2013, and early warning system based on an extensive geodetic monitoring (combination of GNSS, robotic

total station, and a permanent ground-based SAR) has been progressively developed to protect people and infrastructures. The emergency scenario in 2023 gained resonance in the media due to the successful evacuation of the population (ca. 100 people) on May 13th, i.e. ca. 1 month before the failure event. The main goal of this work is to investigate the reliability of the information provided by high spatial and temporal resolution satellite SAR, as well as their potential use in operational near-real-time monitoring and early warning contexts.

2 Dataset

We benefit of the high-resolution SAR imagery acquired from the ICEYE constellation, and of the exceptional availability of independent measurements and ground observations allowing for a thoughtful validation. ICEYE is a commercial operator offering spaceborne SAR imagery (X-Band, 9.65GHz, wavelength 3.1 cm) acquired with different modalities (details can be found at ICEYE, 2024). The current configuration allows covering the Earth's surface ca. every 6 hours, although imaging modes and/or the geometrical characteristics may strongly differ. For our application in Brienz, we considered the imagery acquired in Spot Imaging mode, VV polarization, covering an area of 5 x 5 km. Among the four different views available, the ascending orbit, left looking (ASC_L), provides an optimal sight over the area of interest and minimal zones of layover and shadow (dark/black areas in Fig. 1b), as well as a total of 16 images acquired in the period before the failure event (see Table A1 and Fig.1c, red filled triangles, average revisit time 1.6 days, minimum ca. 25 minutes, maximum 4 days). Incidence angles vary from ca. 17 to ca. 37 degrees (see also Table A1). We used the GAMMA software to initially process the Single Look Complex (SLC) images, applying a multilooking of 2 samples in azimuth and 1 in range, resulting in a ground sapling distance (GSD) of ca. 0.42 m × 0.33 m, in range and azimuth directions, respectively. SAR images were then aligned (co-registered) considering as reference the acquisition on May-22, 2023 (ID1 in Table A1), and then radiometrically terrain corrected (RTC, Small et al., 2022) benefitting of a high-resolution digital topographic surface model openly provided by Swisstopo over entire Switzerland (GSD 0.50 m). The RTC removes the influence of topography on SAR backscatter and ensures an appropriate evaluation its values and of their variations over space and time.

3 Pre-event: measuring accelerated slope deformation.

Pixel-offset (hereafter referred to as PO) is a well-established method to measure displacements in digital imagery. For what concerns SAR imagery, PO is an efficient alternative to radar interferometry to measure displacements when large spatial gradients occur due to landslide processes. We adapted the PO method presented in Bickel et al., (2018) by first converting the SAR backscatter in an orientation image (Dematteis and Giordan, 2021). We used a template window of 128×128 pixels, overlap 75%, and oversampling factor of 4. We computed PO in SAR coordinates (range and azimuth directions) for all possible pairs with images acquired between May-22 and Jun-15, 2023. Then, we converted the results to meters, calculated the magnitude of the 2D surface displacement vectors, and finally generated velocity maps in m/day.

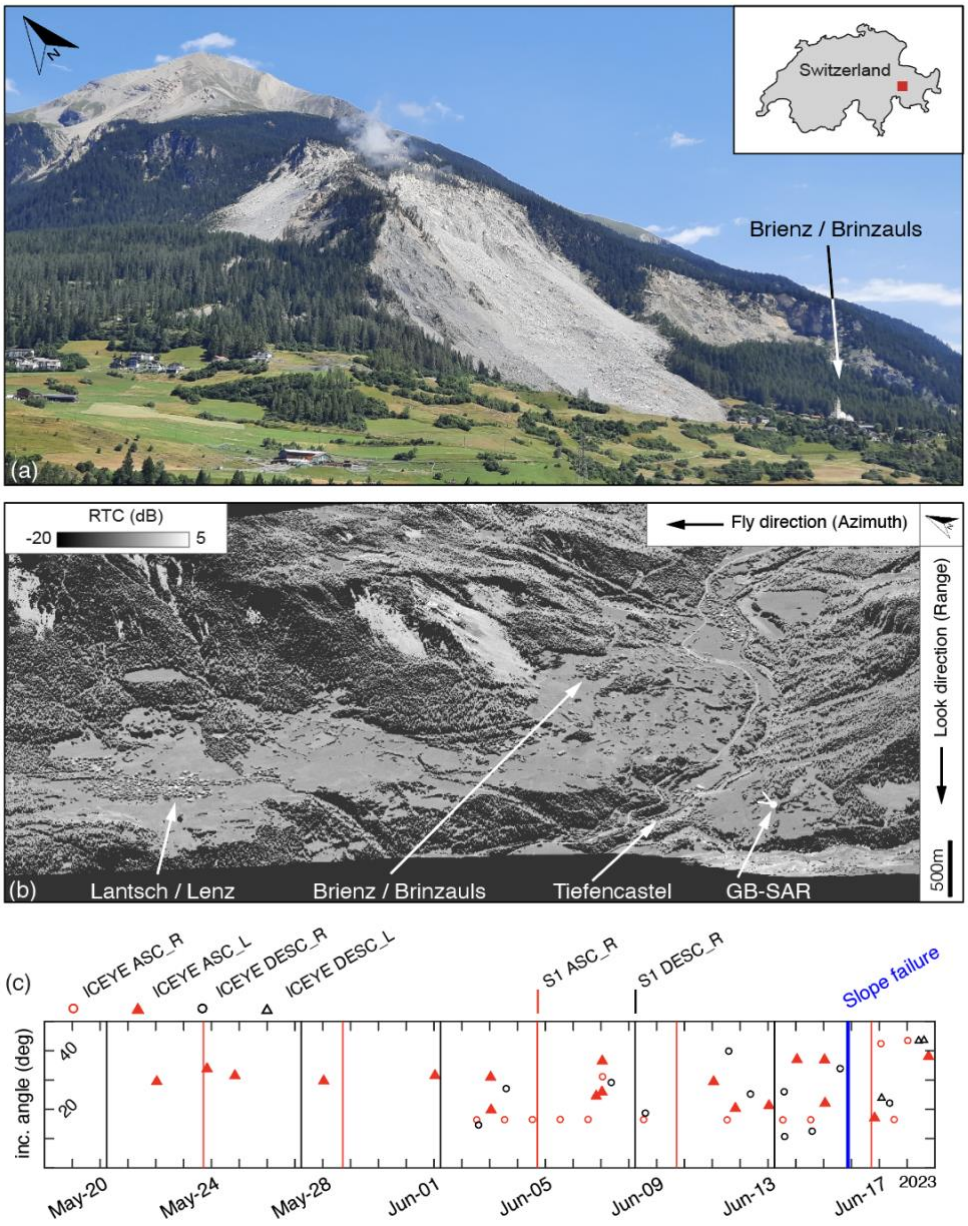

Figure 1: (a) Picture of the Brienz slope acquired from the GB-SAR station (see location in panel 1b) after the failure occurred on Jun-15, 2023. (b) Reference SAR (May-22, 2023) backscattering image in dB, after radiometric terrain correction. Some points of interest are indicated for spatial orientation. (c) Sentinel-1 and ICEYE imagery acquired over Brienz with indication of orbit direction (ascending or descending) and sensor look direction (left or right).

The velocity results for selected snapshots are shown in Fig 2. The acceleration of the portion failed on June-15, called the Island, is clearly visible compared with the rest of slope. There, velocities increased from about 0.25 m/day reported on May-28, to a maximum of 0.5 m/day on June-03, 2023 (Fig. 2a). Thereafter, the values reached ca. 1 m/day on Jun-11 and then ramped up to maximum values of 4 m/day on Jun-15, i.e., the day of the failure.

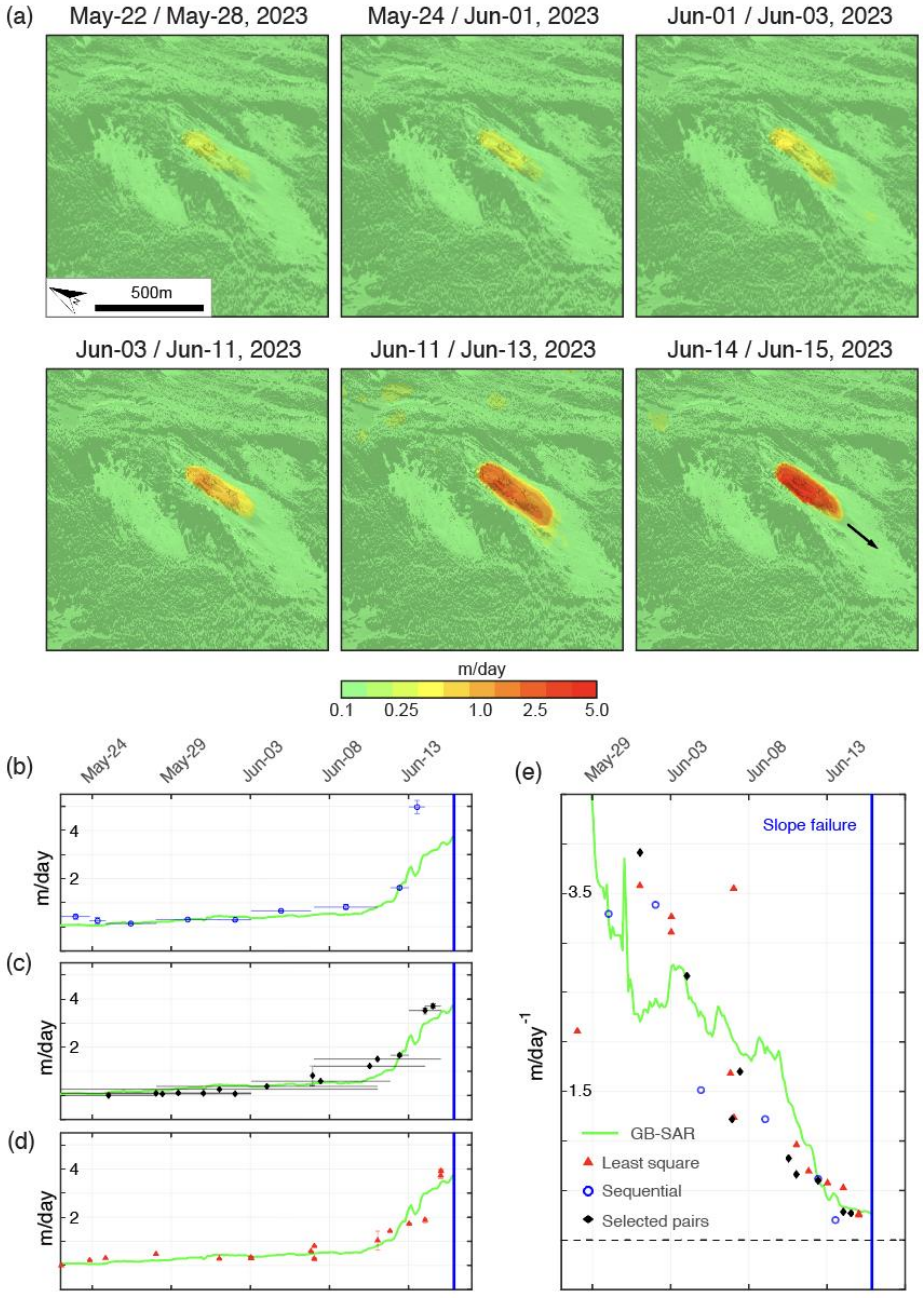

Figure 2: (a) Selected results showing the 2D surface velocities over Brienz measured with pixel-offset (PO) applied to the ICEYE data. Note that the colour scale is logarithmic to show the extreme differences in velocities occurred within few days a factor six larger compared to the one showed in (a). (b-d) Time series of maximum surface velocities measured with PO vs. velocities recorded with GB-SAR. Horizontal bars in b and c show the time span of the images paired. Error bars, in most cases smaller than the symbol size, are related to the median PO measured in an area considered stable (e) Inverse velocity plot to show failure forecasting potential of ICEYE PO results vs. GB-SAR.

We extracted the maximum PO velocities for all pairs and generated velocity time series to compare with the measurements obtained from a Ground-Based (GB) SAR installed in Brienz for early warning purposes and measuring every 4 minutes. Fig. 2b shows the comparison between three different approaches to generate the time series from the PO results and the GB-SAR measurements. For all three time series approaches, we considered the statistical distribution of PO velocities obtained in a stable area 1'000 x 1'000 pixels (i.e., 420 m x 330 m) to estimate the inaccuracies, which are in most cases below 0.1 m/day (see error bars in Fig. 2b). For the first time series approach, we computed PO versus the first available subsequent image (i.e., sequential), without any constraints on the view angles, but considering at least 1day of temporal baseline. The results agree with the GB-SAR time series with a RMSE of 0.06 m (see Table A2) when the last pair close to the failure time is not considered. Such deviation is caused by the large differences in incidence angle between the images (almost 15 degrees between image ID13 and ID14, Table A1). For this reason, in the second time series approach we used all possible PO pairs with at least 24 h temporal baseline, but also constrained incidence angle differences to max 1.5 degrees. This value was fixed after several trials and allowed preserving enough pairs and high signal-to-noise ratio in the PO results. The results show a very good match with the GB-SAR over the entire time series (RMSE 0.08 m), showing the high potential of ICEYE in monitoring applications in case acquisition parameters would be nearly constant over the area of interest. Finally, as third approach we used the least square optimization to compute displacement time series (Casu et al., 2011), also in this case by considering acquisitions with incidence angle differences lower than 1.5 degrees. Also in this case, the results compare well with the GB-SAR velocities (RMSE 0.01 m), with the advantage that the velocities are estimated at the dates of acquisition and not representative of an average value in between the pairs, as for the two other methods.

Fig. 1c shows the conversion of the velocity time series into their inverse. When velocity increases exponentially, its inverse approaches progressively lower values, and the linear projection of the time series to zero is expected to provide an indication of the ultimate stages towards an impending slope failure (Fukuzono, 1985). Despite different versions and ad-hoc adaptations developed over the years, the inverse velocity approach is widely used in operational scenarios to infer the time of slope failure and to manage early warning scenarios (Sharifi et al., 2024). Our results show that the inverse velocity values retrieved from PO applied to the ICEYE images and the GB-SAR time series converge comparably towards the failure occurred on Jun-15, 2015. This suggests that the increase in spatial and temporal resolution of space borne SAR datasets can provide new solutions for continuous monitoring when in-situ datasets are not available, and potentially be used in operational early warning scenarios to forecast time-of-failure.

4 Post-event: slope failure documentation and volume estimation.

Optical and radar images are often used in the events aftermath to document and characterize the slope failure in terms of area and assets affected by the failed materials and to study the runout dynamics (Guzzetti et al., 2012).

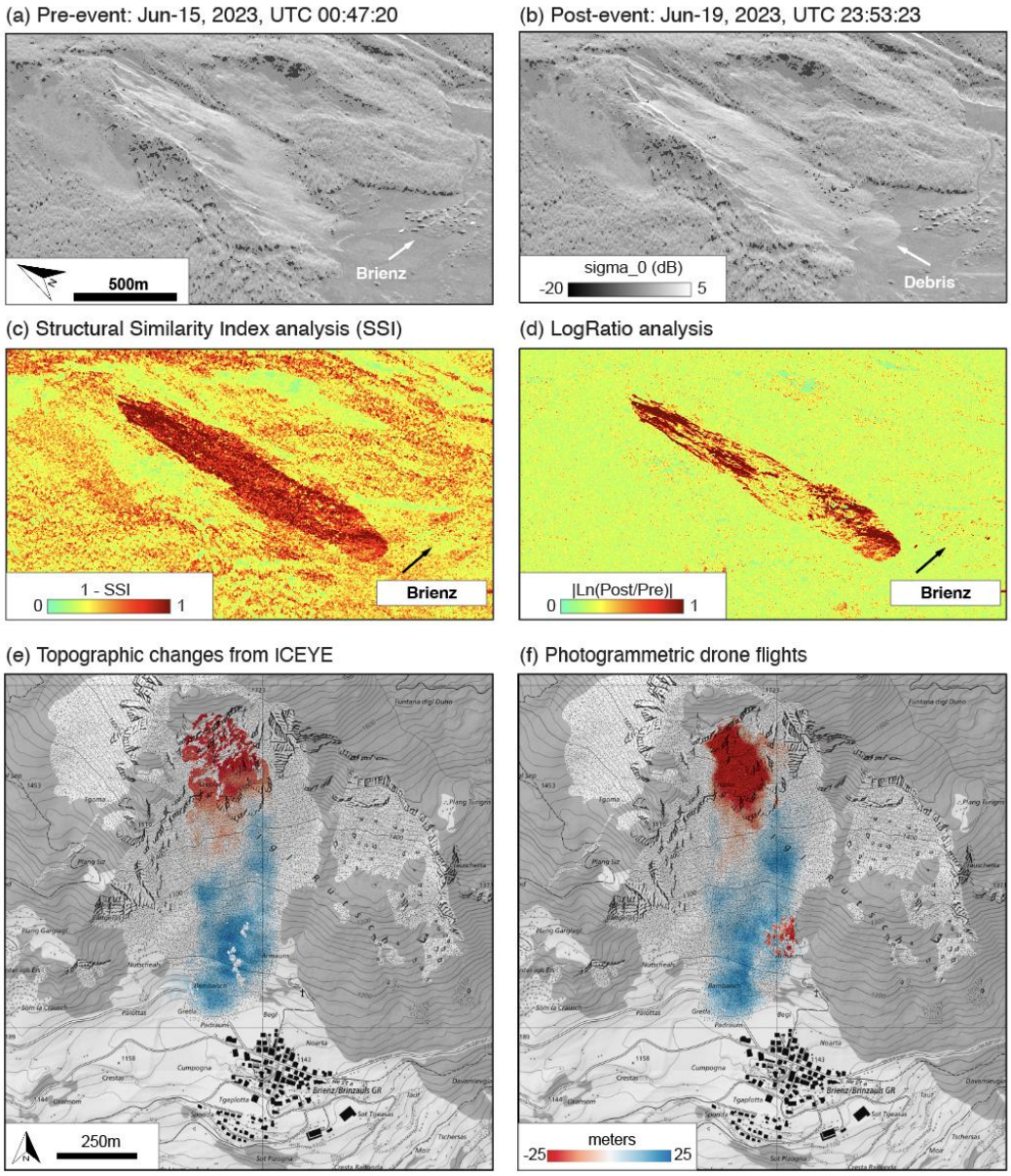

Figure 3: Comparison between (a) pre- and (b) post- event ICEYE images acquired over Brienz. (c) and (d) show the results of analytical change detection attempts with SSI and log-ratio methods, respectively. Comparison between (e) ICEYE interferometry and (f) DSM-of-Difference (DoD) generated from photogrammetric drone flights. Note that the negative height difference in (f) in the lower part above the village are trees cut down by the landslides.

In Fig. 3a and 3b, we show pre- and post-event ICEYE Spot images backscattering, which already allow to visually identify areas affected by changes (erosion and deposition) as well as assets invaded by the debris materials (i.e., the cantonal road connecting Brienz to the village of Lantsch/Lenz, see Fig. 1).

Change detection computation, such as for example the Structural Similarity Index (SSI (Wang et al., 2004)) or the log-ratio (Mondini, 2017) applied to the backscattering (shown Fig. 3c and 3d, respectively) can be used efficiently to map landslide boundaries and highlight important features associated to the failure dynamic, by benefitting of the high spatial resolution. However, change detection provides only a 2-dimensional view of the event characteristics. To estimate the volume of the failed material, photogrammetric approaches based on space- or airborne optical imagery, as well as terrestrial and airborne LiDAR, are generally used due to their flexibility and high-resolution results on the reconstruction of surface topography. Spaceborne SAR can be also used for identification of topographic changes, provided that SAR scenes are acquired with the same orbit and view angles, and that perpendicular baselines (i.e., orbit separation) between images acquired before and after the event remain within critical values for the determination of heights with interferometry (Bürgmann et al., 2000). Among the dataset we considered, two ICEYE images acquired after the Jun-15 event in Brienz (i.e. on Jun-18 and Jun-22, 2023, ascending orbit, right look) have same view angle and a spatial baseline of 931m resulting in a height of ambiguity of 7.6m. The differences between the topography before the failure event and the digital surface models obtained with radar interferometry (InSAR) are shown in Fig.4a. For validation, we compare the InSAR results with a DEM-of-Differences (DoD) obtained after photogrammetric drone flights before (Jun-8, 2023) and right after (Jun-16, 2023) the event (Fig. 4b). The georeferencing accuracy achieved with Post Processing Kinematic (PPK) is in the range of 0.1 m. The spatial distribution of the negative (erosion) and positive changes (deposition) due to the slope failure are well comparable. The 95-percentile of the height differences between InSAR and photogrammetric measurements is in the order of 16 meters, with local peaks up to 50 meters. This leads to the estimated negative volumes from InSAR are -0.79 Mm^3 vs. -1.24 Mm^3 from photogrammetry, i.e. a difference of about 40%. Deviations in the source area are most likely due to phase unwrapping errors (procedure to convert the phase differences retrieved with InSAR into metric scale), associated to the presence of steep slopes and decorrelation due to large phase gradients. Another source of inaccuracy is atmospheric disturbance, as well as surface changes (minor slope failures) that occurred in the upper ranges of the slope after the main event. On the other end, deposited volumes from InSAR are +1.18 Mm^3, very similar to the +1.28 Mm^3 estimated from photogrammetry, only 10% difference.

5 Conclusions and Outlook

Reliable warning systems with high temporal and spatial resolution are the key to prevent life and asset loss caused by slope failure. In Brienz, an exceptional in-situ network allowed to recognize in due time the evolution towards a potential catastrophic failure, supporting the decision of local authorities to evacuate the population and restricting access to areas and infrastructures at risk. However, such an extensive monitoring system is not replicable in all mountain areas where it would be needed, mainly due to logistic/access reasoning and/or financial matters. Satellite data, available in all weather conditions with sub-metric spatial resolutions and sub-daily revisit, can be a viable alternative to manage slope instability operational scenarios. As demonstrated in this work, the results obtained from high resolution SAR images are well comparable with the ground-based monitoring data and could be used also for near-real-time forecasting of time-of-failure with similar outcomes. In addition, the increase in spatial and temporal resolution allows for prompt and accurate post-event mapping of the slope failure and could

support the determination of event magnitudes (volumes) via InSAR. Intrinsic limitations due to the combination of satellite viewing geometries and slope orientation might still hinder the use of such an approach at high elevations. Moreover, in some cases the unavailability of recent, high resolution topographic models might affect the accuracy of geocoding and decrease the quality of the results. Despite that, we have shown that the very high spatial resolution allows working efficiently also in SAR coordinates, as the targets of interest and changes can be clearly identified. Our results provide a step forward towards the use of satellite SAR imagery for operational scenarios, bringing new insights on the use of satellite SAR to monitor and potentially forecast imminent slope failure in operational early warning scenarios. Accurate information provided timely by SAR satellites day and night and in all-weather can be used in data-driven forecast methods as the inverse velocity approach shown here, as well as for the calibration of more sophisticated numerical models aimed at the evaluation of slope stability and/or to simulate runout scenarios (Bartelt et al., 2018; Gaume et al., 2024).

Appendix

ID	Date & Time (UTC)	Time difference (days)	Inc. angle (degrees)
1	2023.05.22 00:50:15	-	29.70
2	2023.05.23 20:12:39	1.8	34.05
3	2023.05.24 20:14:12	1.0	31.70
4	2023.05.28 00:50:34	3.19	29.90
5	2023.06.01 00:47:47	3.99	31.70
6	2023.06.03 00:50:12	2.0	31.17
7	2023.06.03 01:12:45	0.01	19.90
8	2023.06.06 19:51:52	3.77	24.70
9	2023.06.07 00:51:21	0.2	26.12
10	2023.06.07 01:06:24	0.01	36.70
11	2023.06.11 01:11:01	4.0	29.65
12	2023.06.11 19:53:55	0.77	20.50
13	2023.06.13 00:54:14	1.2	21.45
14	2023.06.14 01:03:47	1.0	37.20
15*	2023.06.15 00:47:20	0.98	37.10
16	2023.06.15 01:15:19	0.02	22.27
17	2023.06.16 19:55:26	1.77	17.23
18**	2023.06.18 22:55:43	2.12	43.5
19*	2023.06.19 23:53:23	1.04	35.37
20**	2023.06.22 22:13:03	2.93	43.5

Table A1: List of ICEYE imagery (mode SPOT, Ascending orbit, left looking sensor, VV polarization), date and time of acquisition (format (yyyy.mm.dd HH:MM:SS), relative temporal baselines (in days), and incidence angles. *Images used for detecting change between pre- and post- slope failure, selected due to similarity in incidence angle (see Fig. 3). **Images used for the estimation of topographic changes with radar interferometry (see Fig. 4).

PO Time series method	Min residual (m)	Max residual (m)	RMSE (m)
Sequential*	-0.34	0.11	0.06
Sequential	-2.76	0.11	0.31
Selected	-0.68	0.34	0.085
Least square	-0.47	1.10	0.10

Table A2: Summary table of the differences between the surface velocity time series measured before Brienz failure with GB-SAR and the PO timeseries obtained from ICEYE. Residuals are computed by resampling the GB-SAR time series on the time vector of the specific PO time series. Negative sign in the residual means PO overestimates GB-SAR velocities. Sequential* is referred to as the results without considering the last sample, which is a clear outlier caused by major difference in incidence angles in the last pair.

Data and software availability

The raw ICEYE Spot images used in this study can be downloaded from the ICEYE archive (https://www.iceye.com/lp/iceye-18000-public-archive). The GAMMA software used for the processing of the SAR images is available at https://www.gamma-rs.ch/software. The PO algorithm used in this work is available at https://github.com/bickelmps/DIC_FFT_ETHZ. The digital height models for pre-failure were retrieved from the https://www.swisstopo.admin.ch/en/height-model-swisssurface3d.

Author Contributions

AM conceived the study, processed the ICEYE imagery to generate the PO time series and the change detection analyses, produced the graphics, and wrote the manuscript. YB and AS acquired and processed the photogrammetric drone imagery to compute the volumetric changes shown in Figure 4 and revised the manuscript. JG provided funding resources for the acquisition of the ICEYE images and revised the manuscript. VT and QZ supported the acquisition of the ICEYE images, derived the InSAR results and revised the manuscript.

Competing interests

At least one of the (co-)authors is a member of the editorial board of Natural Hazards and Earth System Sciences.

Disclaimer

(will be included in the published version of the article)

Acknowledgements

We thank Melanie Rankl and Michael Wollersheim from ICEYE Oy for supporting the data acquisition and for fruitful discussions on the results. Two anonymous reviewers provided insightful comments that helped improving the manuscript.

References

Imaging modes | SAR data | ICEYE: https://www.iceye.com/sar-data/imaging-modes, last access: 3 April 2024.

swissSURFACE3D: https://www.swisstopo.admin.ch/en/height-model-swisssurface3d, last access: 3 April 2024.

Bartelt, P., Christen, M., Bühler, Y., and Buser, O.: Thermomechanical modelling of rock avalanches with debris, ice and snow entrainment, in: Numerical Methods in Geotechnical Engineering IX, Volume 2, CRC Press, 2018.

Bianchini, S., Solari, L., Bertolo, D., Thuegaz, P., and Catani, F.: Integration of Satellite Interferometric Data in Civil Protection Strategies for Landslide Studies at a Regional Scale, Remote Sensing, 13, 1881, https://doi.org/10.3390/rs13101881, 2021.

Bickel, V. T., Manconi, A., and Amann, F.: Quantitative Assessment of Digital Image Correlation Methods to Detect and Monitor Surface Displacements of Large Slope Instabilities, Remote Sensing, 10, 865, https://doi.org/10.3390/rs10060865, 2018.

Bürgmann, R., Rosen, P. A., and Fielding, E. J.: Synthetic aperture radar interferometry to measure Earth's surface topography and its deformation, Annual Review of Earth and Planetary Sciences, 28, 169–209, 2000.

Casu, F., Manconi, A., Pepe, A., and Lanari, R.: Deformation Time-Series Generation in Areas Characterized by Large Displacement Dynamics: The SAR Amplitude Pixel-Offset SBAS Technique, IEEE Transactions on Geoscience and Remote Sensing, 49, 2752–2763, https://doi.org/10.1109/TGRS.2010.2104325, 2011.

Dematteis, N. and Giordan, D.: Comparison of Digital Image Correlation Methods and the Impact of Noise in Geoscience Applications, Remote Sensing, 13, 327, https://doi.org/10.3390/rs13020327, 2021.

Figi, D., Thöny, R., Breitenmoser, T., Brunold, F., and Schwestermann, T.: Rutschung Brienz/Brinzauls (GR): Geologisch-kinematisches und hydrogeologisches Modell, 27/2, 1–34, 2022.

Fukuzono, T.: A New Method for Predicting the Failure Time of a Slope, Proc. IVth International Conference and Field Workshop on Landslides, Tokyo, 1985.

Gaume, J., Kenner, R., Bühler, Y., Stoffel, A., Vicari, H., Kyburz, M., Cicoira, A., and Blatny, L.: Blind prediction of the Brienz rock avalanche runout using a 3D Material Point Method., Intrapraevent, Proceedings of, 2024.

Guzzetti, F., Mondini, A. C., Cardinali, M., Fiorucci, F., Santangelo, M., and Chang, K.-T.: Landslide inventory maps: New tools for an old problem, Earth-Science Reviews, 112, 42–66, https://doi.org/10.1016/j.earscirev.2012.02.001, 2012.

Manconi, A.: How phase aliasing limits systematic space-borne DInSAR monitoring and failure forecast of alpine landslides, Engineering Geology, 287, 106094, https://doi.org/10.1016/j.enggeo.2021.106094, 2021.

Mondini, A. C.: Measures of Spatial Autocorrelation Changes in Multitemporal SAR Images for Event Landslides Detection, Remote Sensing, 9, 554, https://doi.org/10.3390/rs9060554, 2017.

Sharifi, S., Macciotta, R., and Hendry, M. T.: Critical assessment of landslide failure forecasting methods with case histories: a comparative study of INV, MINV, SLO, and VOA, Landslides, https://doi.org/10.1007/s10346-024-02237-5, 2024.

Sigmundsson, F., Parks, M., Geirsson, H., Hooper, A., Drouin, V., Vogfjörd, K. S., Ófeigsson, B. G., Greiner, S. H. M., Yang, Y., Lanzi, C., De Pascale, G. P., Jónsdóttir, K., Hreinsdóttir, S., Tolpekin, V., Friðriksdóttir, H. M., Einarsson, P., and Barsotti, S.: Fracturing and tectonic stress drive ultrarapid magma flow into dikes, Science, 383, 1228–1235, https://doi.org/10.1126/science.adn2838, 2024.

Small, D., Rohner, C., Miranda, N., Rüetschi, M., and Schaepman, M. E.: Wide-Area Analysis-Ready Radar Backscatter Composites, IEEE Transactions on Geoscience and Remote Sensing, 60, 1–14, https://doi.org/10.1109/TGRS.2021.3055562, 2022.

Wang, Z., Bovik, A. C., Sheikh, H. R., and Simoncelli, E. P.: Image quality assessment: from error visibility to structural similarity, IEEE Transactions on Image Processing, 13, 600–612, https://doi.org/10.1109/TIP.2003.819861, 2004.